JOURNAL OF APPLIED ELECTROCHEMISTRY 5 (1975) 197–202

High oxide ion conduction in the sintered oxides of the system Bi_2O_3-Gd_2O_3

T. TAKAHASHI, T. ESAKA, H. IWAHARA

Department of Applied Chemistry, Faculty of Engineering, Nagoya University, Nagoya, Japan

Received 1 July 1974

In order to characterize the conduction behaviour in the sintered oxides of the system Bi_2O_3–Gd_2O_3, the electrical conductivity in air and the emf of the oxygen concentration cell were measured.

The new rhombohedral phase found in this system exhibited high oxide ion conduction especially at relatively high oxygen pressure. The rhombohedral phase was stable in the composition range between 10 and 30 mol % Gd_2O_3 below 600°C and was transformed into the face-centred cubic phase with rising temperature, the conduction in which was by oxide ion as in the rhombohedral phase. At concentrations greater than 35 mol % Gd_2O_3, the fcc phase was stable over a wide range of temperature (~ 900°C) and kept its high oxide ion conduction. The conductivities of rhombohedral $(Bi_2O_3)_{0.90}(Gd_2O_3)_{0.10}$ and fcc $(Bi_2O_3)_{0.65}(Gd_2O_3)^*_{0.35}$ are 4·5 and 2·4 × $10^{-2}\,\Omega^{-1}\,cm^{-1}$ at 600°C, respectively. These are about one order of magnitude higher than that of the well-known yttria-stabilized zirconia at corresponding temperatures. High-oxide ion-conduction in the rhombohedral and fcc phase was considered to be due to the appreciable numbers of oxide ion vacancies in these crystals.

1. Introduction

Bismuth sesqui-oxide has four polymorphs [1, 2, 3]. These are α-Bi_2O_3 which is stable below 730°C and has a monoclinic structure, metastable β-Bi_2O_3 which has a tetragonal lattice and two high-temperature modifications, γ- and δ-Bi_2O_3 which have cubic structures. The phase transformation of α-Bi_2O_3 into the δ-phase takes place at 730°C [3]. Several investigators examined the electrical conduction in pure Bi_2O_3 and reported that α-Bi_2O_3 had low *p*-type conductivity, while δ-Bi_2O_3 had high oxide ion conductivity which was attributed to the migration of a number of oxygen ion vacancies present in its defect fluorite type structure [4, 5, 6]. Consequently, the Arrhenius plot of the conductivity of bismuth sesqui-oxide shows the sharp conductivity rise at 730°C due to the phase transformation. This phase transformation is accompanied by a large volume change which makes the specimen collapse. Therefore, Bi_2O_3 is unable to be used practically as an oxide ion conductor.

The present authors reported previously that the sintered oxide of the solid solution based on $3Bi_2O_3 \cdot WO_3$ was a high conductivity oxide ion conductor having the fcc lattice which corresponded to that of the high temperature modification of Bi_2O_3 (δ-Bi_2O_3) [7]. As this material is stable over a wide range of temperature up to 850°C and is not transformed into another phase at lower temperature, the high oxide ion conductivity is retained even below 730°C [7,8]. The authors also examined the electrical conduction of the system Bi_2O_3–Y_2O_3 and found that (1) the sintered oxide of the system Bi_2O_3–Y_2O_3 had a fcc solid solution range which was stable from room temperature to high temperature and (2) this sintered fcc oxide exhibited oxide ion conduction. The conductivity was higher than that of the solid solution based on $3Bi_2O_3 \cdot WO_3$ at the corresponding temperature [9].

R.K. Datta *et al.* observed the presence of a solid solution having the fcc lattice in the system Bi_2O_3–Gd_2O_3 [10]. High oxide ion conduction was expected in this case. It is also worth noting that Gd_2O_3 is a more effective stabilizer of zirconia than calcia or yttria [11]. Accordingly, we investigated the electrical conduction in the system Bi_2O_3–Gd_2O_3.

* The subscripts to the equations are mole fractions.

2. Experimental techniques

2.1. Preparation of the specimens

The specimens were obtained by the solid state reaction, at elevated temperature, between gadolinium sesqui-oxide (99·9%) and bismuth sesqui-oxide which had been prepared by the thermal decomposition of bismuth nitrate (JIS special grade) at 700°C. The appropriate quantities of these powdery raw materials were mixed and the mixture fired at 800–1000°C in air for 10 h. Then the sintered oxides were ground finely and molded with a pressure of 3 tons cm^2 into cylinders (4–6 x 8–12 mm) or disks (13 x 2–3 mm). In order to obtain the best sintered state, the molded samples were fired again in air for 10 h at temperatures somewhat below their melting points as shown in Table 1. The

Table 1. Sintering temperature of $(Bi_2O_3)_{1-x}(Gd_2O_3)_x$

Gd_2O_3/x	*Temperature* (°C)
0·0	750
0·05–0·075	820
0·10–0·15	850
0·20–0·25	900
0·30–0·35	960
0·40–0·45	1040
0·50	1140
0·60	1200

$x \times 100 =$ mol %

sintering temperature was raised as the content of Gd_2O_3 was increased.

2.2. Measurement of ionic conduction

The ionic conduction of the specimens was examined by measuring the electrical conductivity of the cylindrical-shaped specimens using an AC bridge (10 kHz) and the emf of an oxygen concentration cell using the disk specimen as the electrolyte. Conductive silver paste was adopted as the electrode material. The oxygen concentration cell was:

$$O_2\ (P_{O_2}, a)\ Ag\ |\text{specimen disk}|\ Ag\ (P_{O_2}, c)\ O_2,$$

in which $P_{O_2}, a = 0{\cdot}21$ atm and $P_{O_2}, c = 1{\cdot}00$ atm. The details of these experimental methods were the same as those described in the previous papers [7, 8, 9].

The crystal structures of the specimens were identified by X-ray diffraction patterns at room temperature. CuKα radiation was used with a nickel filter. The lattice parameter was calculated from diffraction angles in the 30–80° (2θ) region obtained at a slow scanning speed (1°/4 min^{-1}) using $Pb(NO_3)_2$ as the internal standard.

The densities of several samples were measured at 25°C by the standard pycnometer method using *n*-butanol.

3. Results and discussion

3.1. Structural aspects

The specimens did not exhibit the open pores which allow the penetration of gas. The colour changed from orange to yellow with increasing Gd_2O_3 content.

Fig. 1 represents the X-ray diffraction patterns of the specimens for representative compositions.

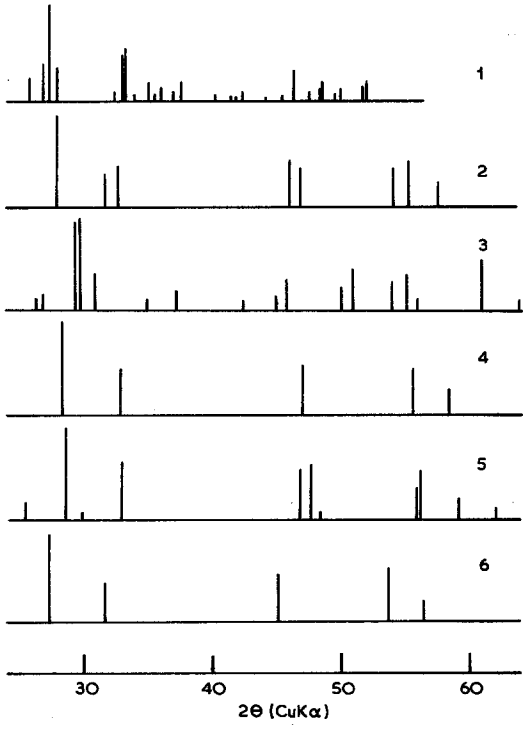

Fig. 1. X-ray diffraction patterns of $(Bi_2O_3)_{1-x}(Gd_2O_3)_x$ cooled slowly from sintering temperature to room temperature. The values for x ($x \times 100 =$ mol %) are: 1-0·0; 2-0·05 (0·05–0·075); 3-0·20 (0·10–0·30); 4-0·40 (0·35–0·50); 5-0·60; 6-δ-Bi_2O_3.

These specimens were cooled slowly from sintering temperature to room temperature in order to avoid the freezing-in of high temperature modifications. Pure Bi_2O_3 shows the characteristic pattern of the monoclinic system. The specimens containing 5, 20 and 40 mol% Gd_2O_3 show the diffraction patterns of the single phase of the tetragonal, rhombohedral and cubic (fcc) system, respectively. Each phase exhibited a solid solution, the composition ranges of which were indicated in the parantheses. However, when the specimens were quenched from sintering temperature to room temperature in a few minutes, even the specimens containing 10 mol% Gd_2O_3 showed the fcc form.

As a result, the fcc phase existed in a wide range of composition (5–50 mol% Gd_2O_3) at high temperature. In the composition range less than 30 mol% Gd_2O_3, the fcc phase was the high temperature phase and this transformed into the tetragonal or rhombohedral phase at lower temperatures. But, in the composition range 35–50 mol% Gd_2O_3, the fcc phase was stable over a wide range of temperature. Though R.K. Datta *et al.* reported the presence of the fcc phase in the composition range 10–50 mol% Gd_2O_3 over a wide temperature range, the present study showed that in the 5–30 mol% Gd_2O_3 range the fcc phase was unstable at low temperatures. It transformed into the tetragonal or rhomobohedral phase as the temperature was lowered.

The phase changes as a function of temperature for various compositions are briefly tabulated in Table 2.

Table 2. Phase change with temperature of $(Bi_2O_3)_{1-x}(Gd_2O_3)_x$

Gd_2O_3/x	*High temperature modification*	*Low temperature modification*
0·05–0·075	fcc	tetragonal
0·10–0·30	fcc	rhombohedral
0·35–0·50	fcc	fcc

$x \times 100$ = mol %

3.2. Ionic conduction

The temperature dependence of the electrical conductivity measured in air for polycrystalline specimens containing Gd_2O_3 concentrations between 5 and 50 mol% is indicated in Fig. 2. The

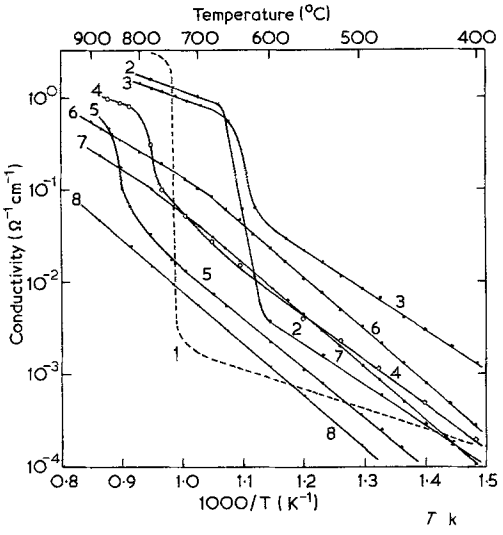

Fig. 2. Conductivity versus reciprocal of absolute temperature curves for $(Bi_2O_3)_{1-x}(Gd_2O_3)_x$ in air. The values for x ($x \times 100$ = mol %) are: 1-0·0; 2-0·05; 3-0·10; 4-0·20; 5-0·30; 6-0·35; 7-0·40; 8-0·50.

conductivity of pure Bi_2O_3 increases with rising temperature and shows an abrupt increase at 730°C corresponding to the phase transformation from a monoclinic into a cubic system. A similar conductivity rise was observed for the sample composition less than 30 mol% Gd_2O_3, but not for composition greater than 35 mol% Gd_2O_3. By means of DTA, the former system was found to exhibit an endothermic process at the temperature at which the conductivity began to rise. Therefore, the abrupt rise of the conductivity observed for the specimens having a tetragonal or rhombohedral lattice at low temperatures was considered to be due to a phase transition into a fcc structure as shown in Table 2. For the Gd_2O_3-rich specimens ($x > 0{\cdot}35$), the single linear correlation observed between log σ and $1/T$ over a wide temperature range suggests that the fcc single phase is stable from room temperature up to 900°C.

In order to determine the charge carriers in these conductors, the oxygen gas concentration cell was constructed using the disk specimen as the electrolyte. Table 3 shows the ratio of the measured emf to the theoretical value when pure oxygen (1 atm) is the cathode gas and air (1 atm) is the anode gas. This ratio is above 0·95 in all cases and independent of the phase transformation. The conductivity measured under various oxygen partial pressures between 1 and $\approx 10^{-5}$ atm coincided with

Table 3. Ratio of the measured emf (E) to the theoretical value (E_0) of the following cell: O_2(0.21 atm), Ag | $(Bi_2O_3)_{1-x}(Gd_2O_3)_x$ | Ag, O_2(1.0 atm)

	E/E_0		
Gd_2O_3/x	600°C	700°C	800°C
0.10	1.00	1.00	1.00
0.20	0.99	0.98	0.98
0.35	0.95	0.95	0.95
0.40	0.99	0.98	0.95

$x \times 100 =$ mol %.

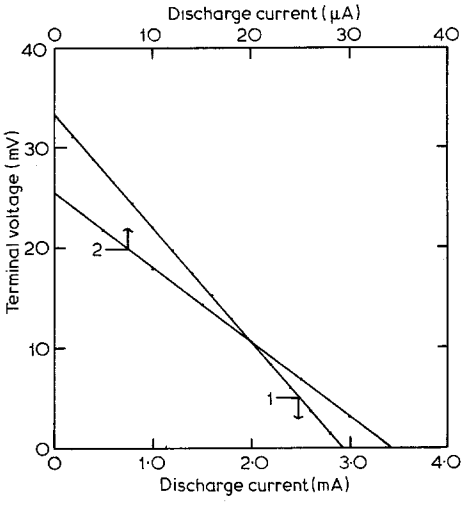

Fig. 3. Terminal voltage versus discharge current relations for the following cell:
O_2(0.21 atm), Ag | $(Bi_2O_3)_{0.65}(Gd_2O_3)_{0.35}$ | Ag, O_2(1·0 atm).
1 - at 760°C; 2 - at 500°C.

the value in air within ± 2%. These results indicate that the electrical conduction in the specimen can be almost wholly attributed to the oxygen ion for the oxygen partial pressure range described above. Relatively large and stable currents could be drawn from the gas concentration cells as shown in Fig. 3. Fig. 3 shows the measured terminal voltage versus discharge current characteristics of the O_2/air concentration cell using a 35 mol % Gd_2O_3 specimen as the electrolyte. The d.c. conductivity calculated from the linear voltage/current relation is nearly equal to the value measured by a.c. Thus the migrating ion in the sintered specimen of the Bi_2O_3–Gd_2O_3 system was concluded to be the oxide ion.

Conductivity/composition isotherms for the system Bi_2O_3–Gd_2O_3 are illustrated in Fig. 4. In both phases (rhombohedral and fcc phase) the

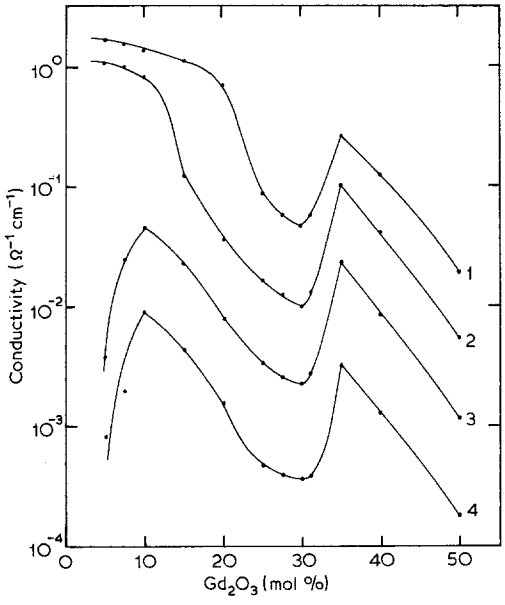

Fig. 4. Conductivity/composition curves for $(Bi_2O_3)_{1-x}(Gd_2O_3)_x$. 1 - 800°C; 2 - 700°C; 3 - 600°C; 4 - 500°C.

oxide ion conductivity decreases with increasing Gd_2O_3 content. It is interesting that in the single phase solid solutions range, the lower the Gd_2O_3 content, the higher the oxide ion conductivity. A similar behaviour has been observed for yttria-stabilized zirconia or yttria-doped thoria.

The results examined above lead to the conclusion that the sintered oxide of the Bi_2O_3–Gd_2O_3 system is an oxide ion conductor. The rhombohedral phase containing 10 mol % Gd_2O_3 and the fcc phase containing 35 mol % Gd_2O_3 have high conductivities of 4·5 and 2·4 × 10^{-2} Ω^{-1} cm^{-1} at 600°C, respectively. These values are higher than the conductivity of yttria-stabilized zirconia by one order of magnitude and are comparable to the high conductivity of the sintered oxide of the Bi_2O_3–Y_2O_3 system.

Lattice parameters of the fcc phase measured by X-ray diffraction showed a linear correlation with composition, see Fig. 5, which coincided with Vegard's rule and indicated that the fcc solid solution was formed over a wide composition range. The densities could be calculated from the above parameters by considering the following four cases.

(1) Ideal cation lattice: the gadolinium atoms occupy some of the cation sites of the defect

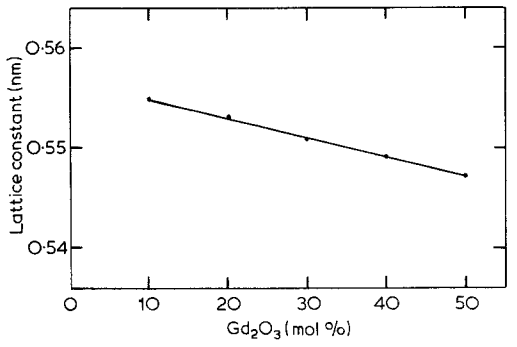

Fig. 5. Lattice constant versus Gd_2O_3 concentration data in the fcc phase of $(Bi_2O_3)_{1-x}(Gd_2O_3)_x$.

fluorite type structure. Therefore, two of eight anion sites in a unit cell are vacant,

$$Bi_{4(1-x)}Gd_{4x}O_6\square_2,$$

where □ represents a vacant oxygen site.

(2) No anion vacancy lattice: the above vacancies are occupied by ionized oxygen.

$$Bi_{4(1-x)}Gd_{4x}O_8.$$

(3) Gd interstitials lattice: the gadolinium atoms occupy the interstitial sites of the bismuth sublattice.

$$Bi_4Gd_{4x/(1-x)}O_{6/(1-x)}\square_{2/(1-x)}.$$

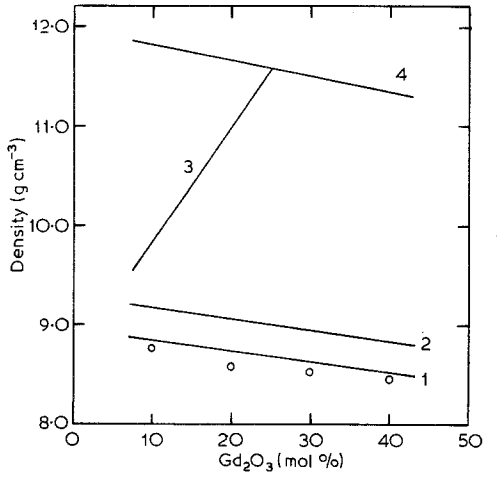

Fig. 6. Comparison of the measured densities (open circles) with the calculated values for various cases. 1 - for case 1: $Bi_{4(1-x)}Gd_{4x}O_6\square_2$; 2 - for case 2: $Bi_{4(1-x)}Gd_{4x}O_8$; 3 - for case 3: $Bi_4Gd_{4x/(1-x)}O_{6/(1-x)}\square_{2/(1-x)}$; 4 - for case 4: $Bi_{4(1-x)}Gd_{4x}(Bi_{4(1-x)/3}Gd_{4x/3})_{int}O_8$.

(4) Ideal anion lattice: the anions occupy their normal sites and the excess cations are situated in the interstitial sites.

$$Bi_{4(1-x)}Gd_{4x}[Bi_{4(1-x)/3}Gd_{4x/3}]_{int}O_8.$$

In these density calculations, as no weight changes were observed during TB, the valencies of Bi^{3+} and Gd^{3+} were considered to be invarient. In Fig. 6, the calculated densities are compared to the observed values. The densities in cases 3 and 4 are obviously different from the observed values. Though the density-composition correlation in case 2 shows a similar tendency to that of the observed, the values are rather high. Moreover, if the vacancies are occupied by ionized oxygen, *p*-type electronic conduction should be introduced as shown by the following equation:

$$V_0^{\cdot\cdot} + 1/2O_2 = O_0 + 2h^+.$$

However, as appreciable electronic conductivity as described above was not observed, case 2 must be rejected.

The measured densities are close to the theoretical values in case 1. As a result, oxide ion vacancies are considered to be present in the fcc phase and high oxide ion conduction in this phase arises in a similar manner to that in the other defect fluorite-type oxides.

The fcc phase in the Bi_2O_3–Y_2O_3 system was reported to be stable at low temperatures because the yttrium atoms occupied not only normal cation sites but also interstitial sites of the cation sublattice [9]. However, according to the above results, the fcc phase in the system Bi_2O_3–Gd_2O_3 has no interstitials. Therefore, the reason why the fcc phase containing more than 35 mol % Gd_2O_3 is stable at low temperature, is not explained by analogy with the Bi_2O_3–Y_2O_3 system. It may be due to the effect of the difference of cationic radius ($r_{Y^{3+}} < r_{Gd^{3+}}$) which is now under investigation in our laboratory.

The rhombohedral phase has not been reported for pure Bi_2O_3. This structure has been confirmed for the systems Bi_2O_3–SrO, Bi_2O_3–La_2O_3 and Bi_2O_3–Sm_2O_3 [12, 13]. As the cationic radius of Gd^{3+} is comparable to that of Sm^{3+}, the rhombohedral phase may exist in the present oxide system. L.G. Sillen *et al.* determined the crystal structure of the rhombohedral phase in the system Bi_2O_3–SrO [13], the X-ray diffraction pattern of which corresponded to the X-ray data of the present

Table 4. Unit cell parameters of the rhombohedral phase of $(Bi_2O_3)_{1-x}(Gd_2O_3)_x$

Gd_2O_3/x	aA^{-1}	$\cos\alpha$	VA^{-3}
0.15	9.489	0.9128	125.13
0.20	9.422	0.9114	124.51
0.25	9.378	0.9111	123.19

$x \times 100 =$ mol %.

system. The lattice parameters were calculated with the aid of the Miller indices (h, k, l) obtained by Sillén. Some of these are listed in Table 4 together with the unit cell volumes calculated. By analogy to Sillén's results, the unit cell was considered to be built up with three cation sites and six anion sites. If gadolinium atoms occupy the equivalent positions to bismuth atoms, the unit cell is formulated as:

$$Bi_{3(1-x)}Gd_{3x}O_{4.5}\square_{1.5}.$$

In Table 5, the measured and the theoretical densities are listed. The measured densities are in good agreement with the theoretical values calculated by the above formula. Consequently, oxide ion vacancies exist in the rhombohedral phase as well as in the fcc phase and probably contribute to the high oxide ion conductivity of the rhombohedral phase.

4. Conclusions

The sintered oxides of the system Bi_2O_3–Gd_2O_3 were found to be oxide ion conductors having negligibly low electronic conductivity under ordinary oxygen partial pressure. The rhombohedral and the fcc single phases in particular exhibited high conductivities which were one order of magnitude higher than those of well-known stabilized zirconias at corresponding temperatures. In this oxide system, the fcc phase was stable for Gd_2O_3 concentrations between 35 and 50 mol % over a wide temperature range up to 900°C, while for less than 30 mol % Gd_2O_3, the low temperature phase (tetragonal or rhombohedral) was transformed into the fcc phase

Table 5. Sample densities of the rhombohedral phase of $(Bi_2O_3)_{1-x}(Gd_2O_3)_x$

Gd_2O_3/x	$d_1/(g\,cm^{-3})$	$d_2/(g\,cm^{-3})$	$d_0/(g\,cm^{-3})$
0·15	8·965	9·284	8·93
0·25	8·897	9·221	8·86

d_1; theoretical density for $Bi_{3(1-x)}Gd_{3x}O_{4.5}\square_{1.5}$.
d_2: theoretical density for $Bi_{3(1-x)}Gd_{3x}O_6$.
d_0: measured density.
$x \times 100 =$ mol %.

with rising temperature; this was accompanied by an abrupt rise of conductivity. The oxide ion conductivities in the rhombohedral and the fcc single phases increased with decreasing Gd_2O_3 contents.

High oxide ion conduction in the rhombohedral phase could be attributed to the migration of oxide ions via oxide ion vacancies as in the case of the oxide ion conduction in the fcc phase, because an appreciable number of oxide ion vacancies were indicated by density measurements in both phases.

References

[1] G. Gattow, *Z. anorg. allgem. Chem.* **298** (1959) 64.
[2] G. Gattow and H. Fricke, *Naturewissenschaften* **48** (1961) 620.
[3] G. Gattow and H. Scröder, *Z. anorg. allgem. Chem.* **318** (1962) 176.
[4] M. G. Hapase and V. B. Tare, *Indian J. Pure Phys.* **5** (1967) 401.
[5] R. S. Sethi and H. C. Gaur, *Indian J. Chem.* **3** (1955) 177.
[6] C. N. R. Rao, G. V. Subba Rao and S. Ramdas, *J. Phys. Chem.* **73** (1969) 672.
[7] T. Takahashi and H. Iwahara, *J. Appl. Electrochem.* **3** (1973) 65.
[8] E. I. Speranskya, *Neorg. Mater.* **6** (1970) 149.
[9] T. Takahashi, H. Iwahara and T. Arao, submitting to *J. Appl. Electrochem.*
[10] R. K. Datta and J. P. Meehan, *Z. Anorg. allgem. Chem.* **383** (1971) 328.
[11] H. Tannenberger *et al.*, *Proc. Int. Etude Pile Comf.* **1** (1965) 13.
[12] E. M. Levin and R. S. Roth, *J. Research N.B.S.* **68A** (1964) 199.
[13] L. G. Sillén and B. Aurivillius, *Z. Krist.* **101** (1939) 483.